RSC Advances

PAPER

View Article Online
View Journal | View Issue

Cite this: *RSC Adv.*, 2018, **8**, 34094

Pure phase synthesis of Cu_3PS_4 and Cu_6PS_5Cl for semiconductor applications†

Brian Graeser and Rakesh Agrawal *

Received 23rd July 2018
Accepted 24th September 2018

DOI: 10.1039/c8ra06241b

rsc.li/rsc-advances

We have achieved the first reported pure phase synthesis of two new nanoparticle materials, Cu_3PS_4 and Cu_6PS_5Cl. We have achieved this through learning about the potential reaction pathways that $CuCl_2$, P_2S_5, and 1-dodecanethiol can take. This study has shown that the key variable to control is the state of the phosphorus source when the $CuCl_2$ is added. If P_2S_5 is added together with the $CuCl_2$ to dodecanethiol then the reaction will follow a path to Cu_3PS_4, but if it is dissolved in dodecanethiol prior to the addition to $CuCl_2$ then the reaction will produce Cu_6PS_5Cl. The formation of these two different phases can occur simultaneously, yet we have found sets of conditions that manipulate the reaction system to form each phase exclusively. These nanoparticles could have broad semiconductor or solid electrolyte applications.

There is a need to explore new thin film photovoltaic absorbers, as many of the current thin film technologies have challenges associated with them. The high efficiency materials such as $CuIn_xGa_{1-x}Se_2$ (ref. 1–5) and CdTe,[6–8] require the use of the less-abundant elements indium and tellurium. To rectify this short coming, materials that use earth abundant elements such as $Cu_2ZnSnSe_4$ (CZTSe)[9,10] and amorphous-Si[11–13] have been explored. This class of materials has been unable to reach the efficiencies of the $CuIn_xGa_{1-x}Se_2$ and CdTe cells that are necessary to become an economic alternative to fossil fuel based energy. Specifically in the case for CZTSe, the issue is caused by intrinsic defect formation, leading to band tails in the material.[14–17] This defect is caused by the zinc on copper site (Cu_{Zn}) and the accompanying copper on zinc (Zn_{Cu}) site.[18,19] This is due to the similar sizes of the Cu^{1+} and the Zn^{2+} ions.

Because of the uncertainties regarding the limitations and future of previously developed earth abundant materials for solar cells, it is necessary to investigate new materials that avoid the pitfalls that have hampered the previous technologies. It has been proposed to use a Cu_3–V–VI_4 (V = P, As, Sb; VI = S, Se) structured material to address these issues.[20–28] This class of materials uses earth abundant cations to allow for production on a terawatt scale. They also avoid the cation switching that has hampered the efficiencies of CZTSe devices, due to the mismatch between the sizes of V^{5+} and Cu^{1+} cations.

Some work examining the phosphorus member of the Cu_3–V–VI_4 material family and its potential use as a solar absorber material has been reported in the literature. The reported calculations have estimated that the band gap of the selenide material is within the ideal range of 1.0–1.5 eV, and they have potential for the power conversion efficiencies to be greater than that of $CuInSe_2$. Experimental studies have confirmed the band gap of Cu_3PSe_4 to be 1.35 eV.[22] On the other hand, Cu_3PS_4 with a higher band gap is a potential candidate for a top cell in a tandem cell. Both of the materials have shown a photoelectric response,[22,23] and could be attractive materials for photovoltaic devices.

In the past, crystals of Cu_3PS_4 have been synthesized either using chemical vapor transport and temperatures in excess of 850 °C for long periods of time such as 24 hours[20,29] or heating elemental powders of copper, phosphorus and sulfur in sealed evacuated fused silica tubes at high temperatures for extended time periods.[22,27,30] While these techniques produce crystals of Cu_3PS_4 that could be used for fundamental characterization, they are not suitable for fabrication of thin films of Cu_3PS_4. There is a need to pursue and develop new solution based techniques for the synthesis of Cu_3PS_4, if it is to be competitive with other thin film technologies. Using nanoparticles as a method for forming thin films has been employed for a variety of other materials for PV applications.[1,9,31,32]

The previous solution-based method, to synthesize Cu_3PS_4 nanoparticles has faced significant obstacles.[23] This method is based on reducing both copper and phosphorus to a neutral state and reacting them together to form Cu_3P nanoparticles. These nanoparticles are then reacted with thiourea in a separate reaction. While this procedure does produce Cu_3PS_4 nanoparticles, they are not pure phase. There is the presence of a phosphorus rich phase that is altering the composition and effecting the photoluminescence. If Cu_3PS_4 nanoparticles are to be used a precursor to a solar absorber, they will need to be free of any contaminants that could adversely affect a final film.

Davidson School of Chemical Engineering, Purdue University, 480 Stadium Mall Drive, West Lafayette, IN 47907, USA. E-mail: agrawalr@purdue.edu

† Electronic supplementary information (ESI) available. See DOI: 10.1039/c8ra06241b

For this contribution we have examined copper–phosphorus–sulfide system. This material can occur in two main phases, the Cu_3PS_4 enargite phase and the Cu_7PS_6 argyrodite phase. The argyrodite structure also has a chloride phase compound Cu_6PS_5Cl. The enargite phase is of more interest for photovoltaic applications, as either a top material for a multi-junction device or for use in high band gap electronic devices.

Argyrodites, while they may not be useful as solar absorbers, have been explored for use as solid electrolytes.[33–35] Cu_6PS_5Cl has been of particular interest due to its high performance and copper mobility.[36,37] This material has shown better conductivities than other materials in the same family. In a similar case to the enargite materials, synthesis of the argyrodites is done in sealed ampule or vacuum based methods.[34–37]

Experimental

Co-addition of $CuCl_2$ and P_2S_5 powders at room temperature for solvothermal nanoparticle synthesis

In a nitrogen filled glovebox, copper(II) chloride (Sigma-Aldrich, ≥99.995% trace metals basis, $CuCl_2$) and phosphorus pentasulfide (Acros Organics, 98+%, P_2S_5) are added to a reaction flask in either stoichiometric amounts or 50% excess phosphorus (Cu : P 2 : 1) content followed by 4 mL of 1-dodecanethiol (Sigma-Aldrich, ≥98%, DDT). This flask is heated to 250 °C under an argon atmosphere and held at that temperature for 1 hour. Then the flask is allowed to cool to room temperature in ambient conditions. After nanoparticles reach room temperature, they are dispersed in a hexane and isopropanol mixture (V : V 1 : 5) and precipitated using centrifugation at 14k rpm for 5 minutes. This washing is done three times and afterwards the nanoparticles are dried under dry nitrogen.

Phosphorus pentasulfide pre-dissolution nanoparticle reaction

P_2S_5 and 1-dodecanethiol are added to a reaction flask under a nitrogen atmosphere, and the flask heated under an argon atmosphere to 250 °C and is held for 1 hour. Then it is cooled to ambient temperature. The flask is opened in a nitrogen atmosphere, and $CuCl_2$ is added to the flask, which is resealed. The flask is heated to 250 °C under argon and is held for 1 hour, then is cooled to room temperature. The particles are dispersed in a hexane and isopropanol mixture (V : V 1 : 5) and are precipitated out by centrifuging at 14k rpm for 5 min. This is done three times, and then the nanoparticles are dried in nitrogen.

Characterization

X-ray diffraction data was gathered using a Rigaku SmartLab diffractometer with a Cu Kα X-ray source. Raman spectra were acquired using a Horiba/Jobin-Yvon LabRAM HR 800 confocal microscope with a 633 nm He:Ne laser. Samples for XRD and Raman spectroscopy were made by drop casting the particles in hexane onto soda-lime glass. UV-Vis was collected by an Agilent Technologies Cary 60 spectrophotometer. Scanning electron microscopy energy dispersive X-ray spectroscopy data (SEM-EDS). Transmission electron microscopy (TEM) for the Cu_3PS_4 nanoparticles was done on a Hitachi 2700-C, and for the Cu_6PS_5Cl nanoparticles s FEI Talos F200X was used.

Results and discussion

We wanted to design a single pot synthesis to simplify the Cu_3PS_4 synthesis and to avoid complications from having multiple steps. For this material in particular there have been issues with residual phosphorus staying on the nanoparticles after an earlier reaction that stays with the nanoparticles through subsequent reactions. Other reaction pathways that use multiple steps could have possibilities for other impurities to be left behind. This means that we need to have our copper, phosphorus, and sulfur source all present and active in our initial reaction.

Synthesis of Cu_3PS_4

We synthesized pure phase Cu_3PS_4 nanoparticles by the novel co-addition of $CuCl_2$ and P_2S_5 powders (Cu : P 2 : 1) at room temperature for nanoparticle synthesis method. The PXRD and Raman spectra are shown in Fig. 1. All peaks seen in those spectra can be assigned to Cu_3PS_4. The phase purity of nanoparticles was confirmed by Rietveld refinement (see ESI†), which found no evidence of the presence of Cu_6PS_5Cl and did not find any unexplained peaks. The composition for the nanoparticles was examined through SEM-EDX (see Table 1), and it showed that the nanoparticles are very close to the expected composition but are slightly phosphorus rich and copper poor. The near stoichiometric composition of 3 : 1 Cu : P produced by this synthesis demonstrates an improvement over the 1 : 1 Cu : P ratio seen in previous studies.[23] This extreme phosphorus excess was hypothesized to be caused by a presence of elemental phosphorus on the surface of the nanoparticles. We attribute the lack of the extra phosphorus in our synthesis to the final solubility of the P_2S_5 in the dodecanethiol. Since the P_2S_5 remained soluble at room temperature any excess can be removed with the solvent using a washing step. Typically this washing is done using isopropanol to remove any excess species from the nanoparticles.

Synthesis of Cu_6PS_5Cl

We were also able to synthesize pure phase Cu_6PS_5Cl nanoparticles by the phosphorus pentasulfide pre-dissolution nanoparticle reaction. The amount of P_2S_5 pre-dissolved in DDT and added $CuCl_2$ lead to Cu : P of 2 : 1. The PXRD data in Fig. 1 matches known spectra for this material. When this spectra was examined using Rietveld refinement, it reported >99% Cu_6PS_5Cl and <1% Cu_3PS_4. We attribute this to experimental error, as the analysis was placing the peaks only within the noise of the spectra (see ESI†), and no Cu_3PS_4 was observable in the Raman spectra. The SEM-EDS shows that the nanocrystals have approximately the correct atomic ratios of Cu, P, and S. We suspect the particles do not have the exact composition because of a few reasons. This synthesis procedure seems to make copper poor nanoparticles as seen in the Cu_3PS_4

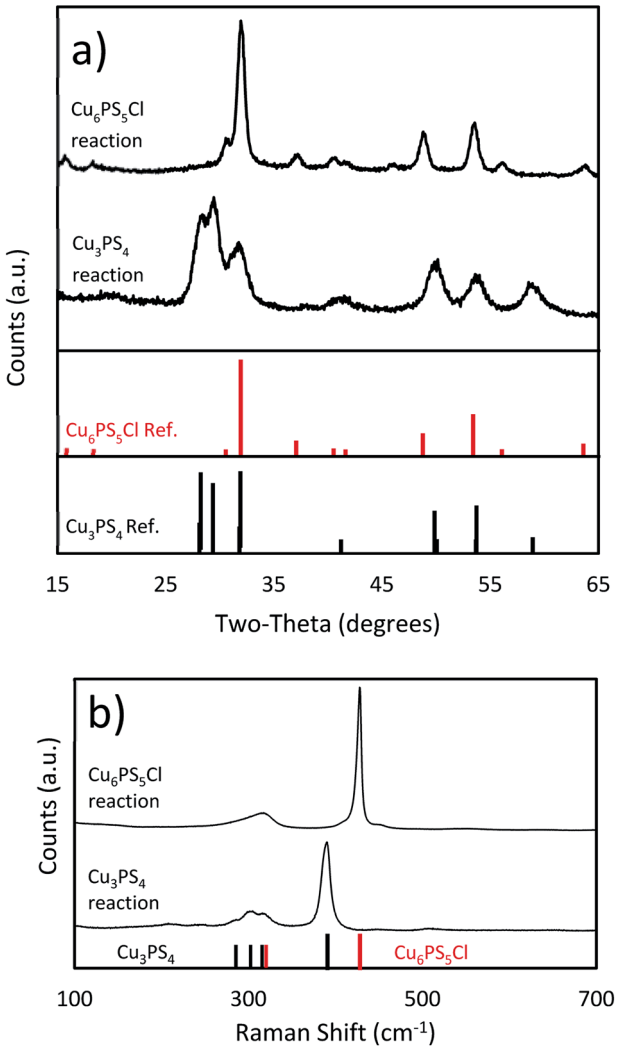

Fig. 1 (a) PXRD spectra (Cu_3PS_4 standard JCPDS: 01-071-3306, Cu_6PS_5Cl standard JCPDS: 01-073-5736) and (b) Raman spectra of the Cu_3PS_4 and Cu_6PS_5Cl nanoparticles.

Table 1 SEM-EDS composition data from the Cu_3PS_4 and Cu_6PS_5Cl nanoparticles, given as elemental ratios with respect to phosphorus

Element	Cu	P	S	Cl
Cu_3PS_4	2.84	1	3.81	0
Cu_6PS_5Cl	5.42	1	5.48	0.44

synthesis, and the dodecanethiol could be attached to the surface of the nanoparticles causing them to be sulfur rich. Being chlorine poor could be explained by a shortage of chlorine in the reaction flask since we know that HCl gas is produced during the initial part of the reaction. We have also taken Raman spectra for this material (see Fig. 1), but we do not have a known standard for it, but based on the previously shown data, we are confident that these nanoparticles are Cu_6PS_5Cl. We will be using this Raman spectra to identify this phase in other samples. The nanoparticles were also examined under

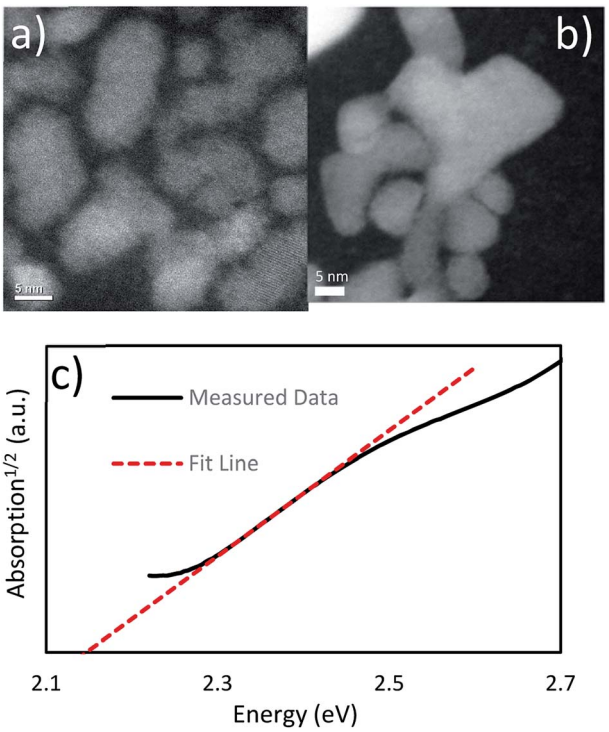

Fig. 2 (a) TEM HAADF image of the Cu_3PS_4 nanoparticles (b) TEM HAADF image of the Cu_6PS_5Cl nanoparticles UV-Vis absorption data for the Cu_3PS_4 nanoparticles shows an indirect band gap at 2.15 eV.

TEM to see their size and shape (see Fig. 2b). The nanoparticles vary widely in shape and size, with sizes ranging from 5–30 nm in calliper diameter. The shapes range from nearly spherical to irregular. The *d*-spacing for these particles was examined from an HR-TEM image and found the correct spacing of 0.28 nm for the {222} plane (see ESI†).

From the TEM images of the Cu_3PS_4 nanoparticles (see Fig. 2a), we can examine their size and shape. We have found them to be about 3–15 nm in diameter and are irregularly shaped. We also examined the plane spacing as well, and found the (002) plane with a *d*-spacing of 0.30 nm (see ESI†). We did not see any evidence of a phosphorus layer on the outside of the nanoparticles. This is in agreement with the SEM-EDX.

The band gap was measured using UV-Vis spectroscopy (see Fig. 2). After examining the absorption$^{1/2}$ curve, we found a linear region that corresponded to an indirect transition at 2.15 eV. It compares favourably with the previous work report for this material having an indirect band gap at 2.3 eV.[20]

Photoluminance data for Cu_3PS_4 also shows the band gap to be around 2.3 eV, close to our measured band gap for nanoparticles synthesized by an earlier method.[23]

The state of phosphorus and how it leads to different reaction products

We have found that the state of the phosphorus source is a determining factor for the nanoparticle phase formed. P_2S_5 reacts with thiols to from thiophosphate esters,[38] and these dissolve in the remaining excess thiol. We have observed the

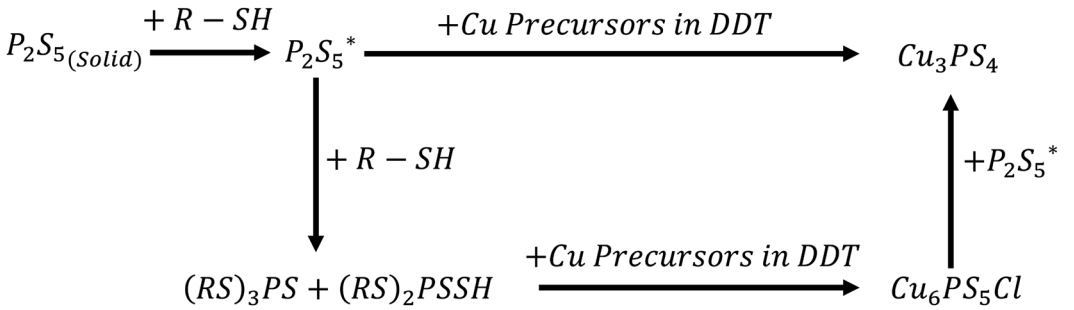

Fig. 3 Proposed reaction scheme for Cu_3PS_4 and Cu_6PS_5Cl syntheses $P_2S_5^*$ is proposed to be the first type of phosphorus species in the solution and is likely a dissolved form of P_2S_5 in thiol at low temperatures. $(RS)_3PS$ and $(RS)_2PSSH$ are likely the second type of phosphorus species formed at higher temperatures.

dissolution of the P_2S_5 to occur in 1-dodecanethiol at elevated temperatures, starting around 100 °C and finishing around 165 °C. Based on this and the other findings shown in this contribution we propose the following reaction pathways for the formation of either Cu_3PS_4 or Cu_6PS_5Cl (see Fig. 3). Different reaction conditions effected the pathway that the reaction would follow and would have a significant impact on the composition of the reaction products. Knowledge of this reaction scheme was what guided us to developing both pure phase syntheses previously described.

To test the significance of the $CuCl_2$ to P_2S_5 ratio, we first added stoichiometric quantities of $CuCl_2$ and P_2S_5 (Cu : P is 3 : 1) to the DDT at room temperature in the flask. This mixture was heated to 250 °C and held there for 1 hour. During heat up, aliquots of samples were collected from the reaction flask and analyzed for composition by Raman spectroscopy, and the results are shown in Fig. 4a. It seems that the reaction of the P_2S_5 with the $CuCl_2$ and DDT happen concurrently. When we compared the two phases of Cu_3PS_4 and Cu_6PS_5Cl nanoparticles present during the heating ramp as well as the final product from the synthesis we saw a shifting composition. As the reaction temperature increased, the Cu_6PS_5Cl phase began to form in a greater amount than the Cu_3PS_4. The final composition was a mixture of both phases.

When the reaction is modified so excess amounts of P_2S_5 are added (Cu : P was 2 : 1) initially at room temperature to the reaction flask, we observed a different end result from the previous stoichiometric case. The beginning of the reaction remained similar with both phases present throughout the reaction period. Although the relative quantity of Cu_3PS_4 was now higher with respect to Cu_6PS_5Cl but then end product was not the same (see Fig. 4b). Due to the excess amounts of P_2S_5 added, all of the Cu_6PS_5Cl phase converted into the Cu_3PS_4 phase. We have tested this conversion in a separate reaction by using Cu_6PS_5Cl as a replacement for the $CuCl_2$ (Cu : P 2 : 1) and observed the phase change to Cu_3PS_4. This occurs at 250 °C but does not happen at 150 °C. The temperature dependence was why the Cu_6PS_5Cl phase appears at low temperatures only to disappear at higher temperatures.

To examine the changes that may occur with the state of phosphorus during the reaction, three experiments were done where the $CuCl_2$ was added to P_2S_5 and DDT mixture at different points in the reaction. While P_2S_5 was added to DDT at room temperature and heated, the $CuCl_2$ with Cu : P of 2 : 1 was added prior to heating, just after reaching 250 °C, and after 1 hour at 250 °C. The composition of the product nanoparticles shifted from Cu_3PS_4 rich to Cu_6PS_5Cl rich as the $CuCl_2$ was added later (see Fig. 5). We suggest that this shift is caused by the reaction history between the P_2S_5 and the DDT. It seems that after P_2S_5 is dissolved in DDT, there are two types of phosphorus species that are present in the solution. The first type reacts with Cu-species to directly form Cu_3PS_4 while the second type reacts to form Cu_6PS_5Cl. At a high temperature of 250 °C, the first type of phosphorus species further reacts with Cu_6PS_5Cl to form Cu_3PS_4. While in this study we have not delineated each type of phosphorus species, it is likely that the first type of phosphorus species are simply dissolved P_2S_5 molecules in DDT (we denote it $P_2S_5^*$ in Fig. 3), and the second type of phosphorus species are by-products of P_2S_5 reaction with DDT such as $(RS)_3PS$ and $(RS)_2PSSH$. An increase in the second type of phosphorus species seems to occur with reaction time at 250 °C leading to favorable formation of Cu_6PS_5Cl over Cu_3PS_4. In another possibility, the reaction of P_2S_5 with DDT may itself provide the two types of phosphorus species.

To isolate the injection process as a possible variable, the synthesis was repeated with DDT heated alone to 250 °C and then injected $CuCl_2$ and P_2S_5 (Cu : P of 2 : 1) powders together at 250 °C. As with the solvothermal reaction in Fig. 4b a time dependent evolution of the composition is seen. The composition shifts from initially being Cu_6PS_5Cl rich to only Cu_3PS_4 over the hour long reaction (see Fig. 6). This demonstrates that when the $CuCl_2$ and the P_2S_5 are added together either at room temperature or at 250 °C, the reaction will eventually produce Cu_3PS_4 free of Cu_6PS_5Cl. However it is interesting to compare initial reaction products in Fig. 4b) at a lower temperature of 150 °C with that in Fig. 6 after 1 minute of injection. We find that while at lower temperatures Cu_3PS_4 is favored, at a high temperature of 250 °C Cu_6PS_5Cl is initially favored. It seems at the temperature of 250 °C, not only the second type of phosphorus species is quick to form but its kinetic rate to form Cu_6PS_5Cl is much higher than corresponding rate with the first type of phosphorus species to form Cu_3PS_4. With co-injection of P_2S_5 and $CuCl_2$ at 250 °C, we have enough first type of phosphorus species to eventually convert all the Cu_6PS_5Cl to Cu_3PS_4.

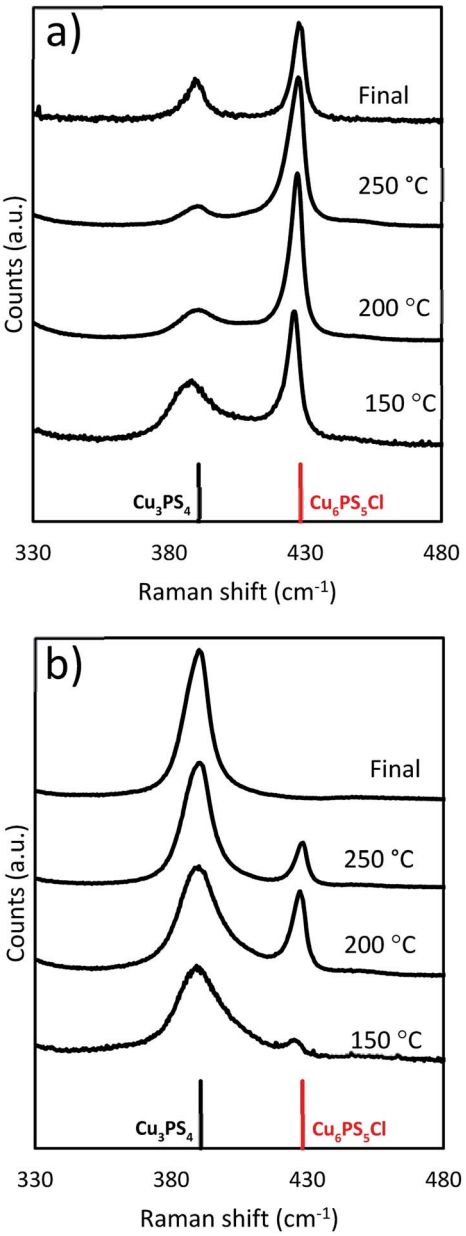

Fig. 4 Raman spectra taken during the temperature ramp for the solvothermal reaction at two different composition loadings, (a) Cu : P 3 : 1, (b) Cu : P 2 : 1. The data at 250 °C represents the sample when the reaction attains 250 °C and the final data is after 1 hour.

The conversion of Cu_6PS_5Cl to Cu_3PS_4

To see if the Cu_6PS_5Cl could directly be converted to Cu_3PS_4, a series of reactions was performed using Cu_6PS_5Cl as the only copper source. These reactions were done under three different conditions. Two that used the solvothermal method, whereby Cu_6PS_5Cl and P_2S_5 are added to DDT at room temperature and the mixture is heated to the reaction temperature of either 150 °C or 250 °C (Fig. 7b and a respectively). In the third experiment, the Cu_6PS_5Cl is added after the P_2S_5 has been heated in DDT for 1 hour at 250 °C (Fig. 7c). The Cu_6PS_5Cl : P_2S_5 in all three experiments was 2 : 3 which is close to the Cu : P

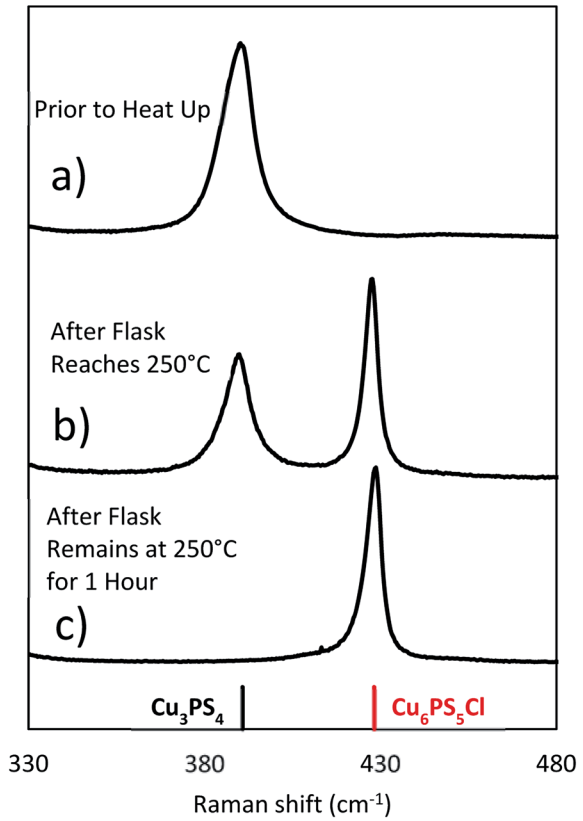

Fig. 5 Final Raman spectra taken after reactions where the $CuCl_2$ is added at different times in the reaction (Cu : P 2 : 1). In (a) the reaction was terminated after 1 hour at 250 °C, while (b) and (c) reactions were terminated after 1 hour following the addition of $CuCl_2$.

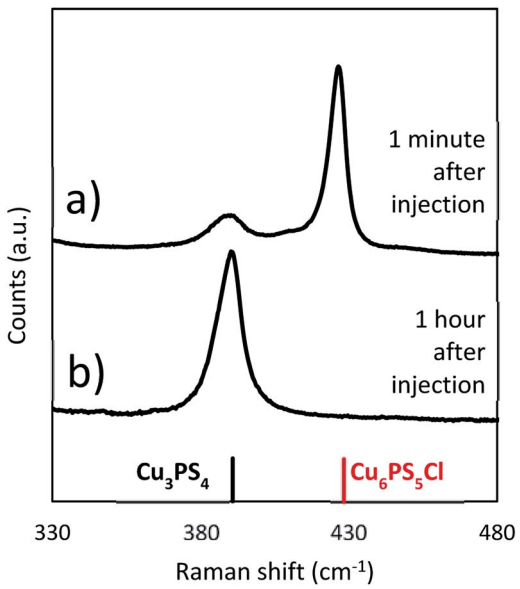

Fig. 6 Raman spectra taken from a synthesis where both $CuCl_2$ and P_2S_5 are both injected as powders at 250 °C (Cu : P 2 : 1) at different points in the reaction (a) 1 minute after injection and (b) 1 hour after injection.

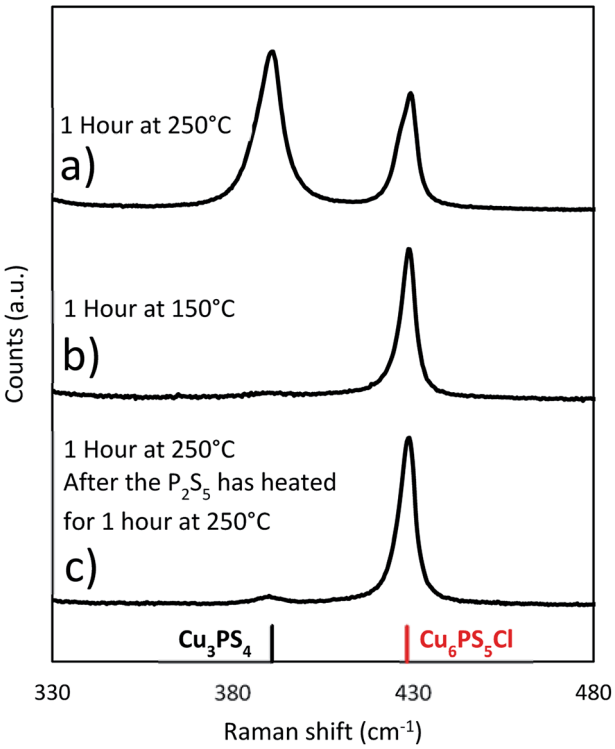

Fig. 7 Raman spectra from reactions where Cu_6PS_5Cl is used as the copper source in place of $CuCl_2$. The Cu_6PS_5Cl is added at room temperature unless otherwise noted. (Cu_6PS_5Cl : P_2S_5 2 : 3).

ratio of 2 : 1 used in earlier experiments. For the solvothermal reactions, there was significant conversion at 250 °C but very little if any at 150 °C (see Fig. 7). This shows that the rate of reaction between the first type of phosphorus species and Cu_6PS_5Cl to form Cu_3PS_4 at lower temperatures (≤150 °C) is quite slower and one needs higher temperatures for this reaction rate to become appreciable. This temperature dependence on the conversion is the reason that in our Cu_3PS_4 synthesis shown in Fig. 4b), Cu_6PS_5Cl is present during early stages of the reaction at lower temperatures and only converts to Cu_3PS_4 later on after the reaction has reached 250 °C. When the P_2S_5 was reacted for an hour with the DDT at 250 °C prior to adding the Cu_6PS_5Cl, the conversion to Cu_3PS_4 was stopped. This is consistent with the possibility that at 250 °C with time there is a decrease in the amount of the first type of phosphorus species and after one hour, the predominant phosphorus species is the second type which does not lead to the formation of Cu_3PS_4. This is consistent with our Cu_6PS_5Cl nanoparticle synthesis recipe where P_2S_5 is first heated at 250 °C in DDT for an hour, the mixture is then cooled to room temperature to add $CuCl_2$ and run the solvothermal synthesis of the nanoparticles.

When the original reaction conditions are used (using $CuCl_2$ and P_2S_5 added together at room temperature to DDT and then heating to reaction temperature and holding for 1 hour) but using temperatures lower than 250 °C, we did not get the desired single phase product (see Fig. 8). We observed similar compositions during the temperature ramp to the previously discussed reactions, where there was a mixture of the Cu_3PS_4 and Cu_6PS_5Cl phases, when the temperature is below 250 °C (Fig. 4b). This was consistent with our findings on the effect of temperature on the conversion from Cu_6PS_5Cl to Cu_3PS_4 and the postulate that there are two types of phosphorus species in the solution with different reaction rates. At lower temperatures, reaction rate between first type of phosphorus species and Cu_6PS_5Cl is low and therefore, one sees a preference for more Cu_3PS_4 as the temperature increases.

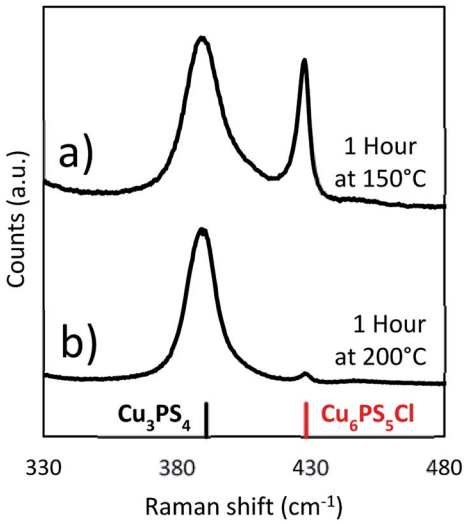

Fig. 8 Raman spectra from solvothermal syntheses at lower temperatures (Cu : P 2 : 1) (a) 150 °C and (b) 200 °C.

Conclusions

Understanding and being able to control the process of the phase change was the important step to achieving each single phase product of Cu_3PS_4 and Cu_6PS_5Cl. High temperatures facilitate the conversion, but it is necessary to add excess P_2S_5 to make sure there is enough phosphorus to complete it. The conversion to Cu_3PS_4 can be completely stopped if the phosphorus is dissolved in the thiol at high temperature of 250 °C before adding the copper, because in this state it will not react with the Cu_6PS_5Cl.

In order to explain the experimental observations and tailor the reaction when P_2S_5 and $CuCl_2$ are reacted in DDT, we invoke the presence of two types of phosphorus species in the solution. The first type of phosphorus species is favoured when excess phosphorus is added to the solution and solution temperatures are low. This first type of phosphorus species reacts directly with copper precursors in the solution to for Cu_3PS_4, and also with Cu_6PS_5Cl to form Cu_3PS_4. Although for the reaction rates to be meaningful with Cu_6PS_5Cl, higher temperatures ($T \sim 250$ °C) are needed. The second type of phosphorus species exclusively reacts with copper precursors in the solution to Cu_6PS_5Cl, and the abundance of this phosphorus species increases as temperature of the reaction is increased. At $T \sim 250$ °C, after a period of about one hour, all of the phosphorus seems to be present as the second type of phosphorus species. It is likely that when P_2S_5 is added to DDT and heated, initial phosphorus

species are of the first type which eventually convert to the second type at the higher temperatures. Once the second type of phosphorus species is present in the solution, it reacts rapidly with copper to form Cu_6PS_5Cl. However, if reaction temperatures are high enough and first type of phosphorus is present in the solution, Cu_6PS_5Cl will react to form Cu_3PS_4. It is likely that the first type of phosphorus is a dissolved P_2S_5 in DDT and the second type of phosphorus species is likely to be formed due to a reaction between P_2S_5 and DDT. Although the possibility of each phosphorus specie to be different by-product of the reaction between P_2S_5 and DDT cannot be ruled out.

Key to producing pure phase Cu_3PS_4 is to ensure the presence of the first type of phosphorous specie and the reaction temperature to be high enough for the conversion of any by-product Cu_6PS_5Cl to Cu_3PS_4. A reaction temperature of 250 °C with co-injection of P_2S_5 and $CuCl_2$ fulfils this condition. It insures that all the by-product Cu_6PS_5Cl is converted to Cu_3PS_4 before the first type of phosphorus species disappears from the solution phase (by perhaps conversion to the second type of phosphorus species). Similarly, pure phase synthesis of Cu_6PS_5Cl requires the absence of the first type of phosphorus species from the solution phase. This is achieved by preheating the P_2S_5 with DDT at 250 °C for one hour. This ensures that there is little of the first type of phosphorus species in the solution phase. Addition of $CuCl_2$ to this solution results in exclusively in the formation of Cu_6PS_5Cl.

In summary, we have shown a new synthesis method for synthesizing copper phosphorus sulfide nanoparticles. Our new synthesis is only a single step reaction that produces a phase pure product, making it advantageous to previous methods that have used multiple reactions and lead to a multiphase product. We have determined that controlling the reaction of the phosphorus pentasulfide with the solvent is the key to determining the phase of the final product. We have tested this using different reaction conditions. These nanoparticles are expected to have applications as a precursor for solar absorber films and other thin-film electronic devices.

Statement of data access

The data associated with this manuscript can be found at the project's website: https://datacenterhub.org/groups/dmref1534691.

Conflicts of interest

There are no conflicts to declare.

Acknowledgements

The authors would like to acknowledge support from NSF grant #1534691-DMR (DMREF: Rabid Design of Earth Abundant Inorganic Materials for Future PVs). The authors would like to thank Caleb Miskin and Xianyi Hu for their assistance with TEM images. The authors would also like to thank Brookhaven National Laboratory for their assistance with the TEM images. The authors like to thank Scott McClary, Joseph Andler, and Caleb Miskin for their helpful discussions.

References

1 S. M. Mcleod, C. J. Hages, N. J. Carter and R. Agrawal, *Prog. Photovoltaics*, 2015, **23**, 1550–1556.
2 P. Jackson, R. Wuerz, D. Hariskos, E. Lotter, W. Witte and M. Powalla, *Phys. Status Solidi RRL*, 2016, **10**, 583–586.
3 T. Todorov, T. Gershon, O. Gunawan, Y. S. Lee, C. Sturdevant, L. Y. Chang and S. Guha, *Adv. Energy Mater.*, 2015, **5**, 1–6.
4 D. Keller, S. Buecheler, P. Reinhard, F. Pianezzi, B. Bissig, R. Carron, F. Hage, Q. Ramasse, R. Erni and A. N. Tiwari, *Appl. Phys. Lett.*, 2016, **109**(15), 152103.
5 R. L. Garris, L. M. Mansfield, B. Egaas and K. Ramanathan, *IEEE J Photovolt.*, 2016, **7**, 281–285.
6 D. Kuciauskas, P. Dippo, Z. Zhao, L. Cheng, A. Kanevce, W. K. Metzger and M. Gloeckler, *IEEE J Photovolt.*, 2016, **6**, 313–318.
7 R. W. Crisp, M. G. Panthani, W. L. Rance, J. N. Duenow, P. a Parilla, R. Callahan, M. S. Dabney, J. J. Berry, D. V Talapin and J. M. Luther, *ACS Nano*, 2014, **8**, 9063–9072.
8 D. E. Swanson, J. R. Sites and W. S. Sampath, *Sol. Energy Mater. Sol. Cells*, 2017, **159**, 389–394.
9 C. K. Miskin, W.-C. Yang, C. J. Hages, N. J. Carter, C. S. Joglekar, E. A. Stach and R. Agrawal, *Prog. Photovoltaics*, 2015, **23**, 654–659.
10 W. Wang, M. T. Winkler, O. Gunawan, T. Gokmen, T. K. Todorov, Y. Zhu and D. B. Mitzi, *Adv. Energy Mater.*, 2014, **4**, 1301465.
11 K. Rudisch, Y. Ren, C. Platzer-Björkman and J. Scragg, *Appl. Phys. Lett.*, 2016, **108**(23), 231902.
12 T. Mise, S. Tajima, T. Fukano, K. Higuchi, T. Washio, K. Jimbo and H. Katagiri, *Prog. Photovoltaics*, 2016, **24**, 1009–1015.
13 T. Matsui, H. Sai, K. Saito and M. Kondo, *Prog. Photovoltaics*, 2013, **21**, 1363–1369.
14 C. J. Hages, N. J. Carter and R. Agrawal, *J. Appl. Phys.*, 2016, **119**(1), 014505.
15 T. Gokmen, O. Gunawan, T. K. Todorov and D. B. Mitzi, *Appl. Phys. Lett.*, 2013, **103**(10), 103506.
16 C. J. Hages, N. J. Carter, R. Agrawal and T. Unold, *J. Appl. Phys.*, 2014, **115**(23), 234504.
17 J. E. Moore, C. J. Hages, R. Agrawal, M. S. Lundstrom and J. L. Gray, *Appl. Phys. Lett.*, 2016, **109**, 1–5.
18 F. Hong, W. Lin, W. Meng and Y. Yan, *Phys. Chem. Chem. Phys.*, 2016, **18**, 4828–4834.
19 K. Biswas, S. Lany and A. Zunger, *Appl. Phys. Lett.*, 2010, **96**, 1–4.
20 J. V. Marzik, a. K. Hsieh, K. Dwight and a. Wold, *J. Solid State Chem.*, 1983, **49**, 43–50.
21 R. B. Balow, E. J. Sheets, M. M. Abu-omar and R. Agrawal, *Chem. Mater.*, 2015, **27**, 2290–2293.
22 V. Itthibenchapong, R. S. Kokenyesi, A. J. Ritenour, L. Zakharov, S. Boettcher, J. Wager and D. Keszler, *J. Mater. Chem. C*, 2013, 657–662.

23 E. J. Sheets, W.-C. Yang, R. B. Balow, Y. Wang, B. C. Walker, E. A. Stach and R. Agrawal, *J. Mater. Res.*, 2015, **30**, 3710–3716.
24 L. Yu, R. S. Kokenyesi, D. A. Keszler and A. Zunger, *Adv. Energy Mater.*, 2013, **3**, 43–48.
25 I. Repins, N. Vora, C. Beall, S.-H. Wei, Y. Yan, M. Romero, G. Teeter, H. Du, B. To, M. Young and R. Noufi, *Mater. Res. Soc. Symp. Proc.*, 2011, **1324**, 97–108.
26 T. Shi, W. Yin, M. Al-jassim, Y. Yan, T. Shi, W. Yin, M. Al-jassim and Y. Yan, *Appl. Phys. Lett.*, 2013, **103**(15), 152105.
27 M. Schulte-Kellinghaus and V. Krämer, *Thermochim. Acta*, 1978, **27**, 141–149.
28 R. B. Balow, C. K. Miskin, M. M. Abu-Omar and R. Agrawal, *Chem. Mater.*, 2017, **29**, 573–578.
29 R. Nitsche and P. Wild, *Mater. Res. Bull.*, 1970, **5**, 419–423.
30 D. H. Foster, V. Jieratum, R. Kykyneshi, D. a. Keszler and G. Schneider, *Appl. Phys. Lett.*, 2011, **99**, 181903.
31 B. K. Graeser, C. J. Hages, W. C. Yang, N. J. Carter, C. K. Miskin, E. A. Stach and R. Agrawal, *Chem. Mater.*, 2014, **26**, 4060–4063.
32 S. A. McClary, J. Andler, C. A. Handwerker and R. Agrawal, *J. Mater. Chem. C*, 2017, **5**, 6913–6916.
33 M. Chen and S. Adams, *J. Solid State Electrochem.*, 2015, **19**, 697–702.
34 W. F. Kuhs, R. Nitsche and K. Scheunemann, *Acta Crystallogr., Sect. B: Struct. Crystallogr. Cryst. Chem.*, 1978, **34**, 64–70.
35 I. P. Studenyak, M. Kranjcec, R. Y. Buchuk, V. O. Stephanovich and S. Kokenyesi, *Semicond. Phys., Quantum Electron. Optoelectron.*, 2013, **16**, 259–264.
36 W. F. Kuhs, R. Nitsche and K. Scheunemann, *Mater. Res. Bull.*, 1979, **14**, 241–248.
37 A. Gagor, A. Pietraszko and D. Kaynts, *J. Solid State Chem.*, 2008, **181**, 777–782.
38 L. Maier and J. R. Van Wazer, *J. Am. Chem. Soc.*, 1962, **84**, 3054–3058.